SUPPLEMENTARY MATERIALS AND METHODS

Histology and Immunohistochemistry

Tissues for immunohistochemistry analysis were harvested at predetermined endpoints (48 hrs or day 38), fixed for 24 hours (4% buffered formalin), transferred to ethanol (70%) and paraffin-embedded. Labels included: Hematoxylin and Eosin (H&E), CD8a primary antibody (1:500; 14-0808, eBiosciences), PDCD1 antibody (MBS175163, MyBiosource, San Diego, CA) and F4/80 (BM8, Biolegend, San Diego, CA). Immunohistochemistry (IHC) was performed manually; antigen retrieval was performed using a Decloaking Chamber (Biocare Medical, Concord, CA) with citrate buffer at pH 6.0, 125 °C and pressure to 15 psi for 45 min. Samples were incubated with primary antibody (room temp, 24 hours) in a humified chamber, where normal goat serum was used for blocking. Next, the secondary antibody, Biotinylated goat anti-rat (1:500; Vector Labs, Burlingame, CA), was used with a Vectastain ABC Kit Elite and a Peroxidase Substrate Kit DAB (both from Vector Labs) used for amplification and visualization of signal, respectively, where the mouse spleen served as a positive control. Lastly, slides were scanned on an AT2 Scanscope (Leica Biosystems) for use with the Imagescope program (Leica Biosystems).

Flow Cytometry Antibodies

Flow cytometry was performed with mouse-specific fluorochrome-conjugated monoclonal antibodies (mAbs). Pacific blue (PB)-anti-CD45 (30-F11), fluorescein isothiocyanate (FITC)-anti-F4/80 (BM8), phycoerythrin (PE) or allophycocyanin (APC)-anti-CD169 (3D6.112), PE-Cy7-anti-CD11c (N418), PE-Cy7-anti-CD3 (145-2C11), APC-Cy7-anti-CD11b (M1/70), Alexa Fluor (AF)-700-anti-Ly6G/Ly6C (Gr-1, RB6-8C5), and AF700-anti-CD8a (53–6.7) were purchased from BioLegend (San Diego, CA). FITC-anti-CD4 (GK1.5) was purchased from BD Biosciences (San Jose, CA). PE-anti-H-2K^{b}-SIINFEKL (25-D1.16) and PE-Cy5-anti-MHCII (M5/114.15.2) were purchased from eBioscience (San Diego, CA). FITC-anti-CD8 (KT15) for use with the tetramer staining panel was purchased from ThermoFisher Scientific (Rockford, IL). IFN-γ secretion from CD8^{+} T-cells was quantified using the Mouse IFN-γ Secretion Assay Cell Enrichment and Detection Kit (130–090-517, Miltenyi Biotec, San Diego, CA) according to the manufacturer's instructions. Negative fluorescence-minus-one (FMO) control staining was performed with isotype-matched mouse, rat or hamster IgG mAbs, and nonspecific binding was blocked with the FcγIII/II receptor-mediated anti-CD16/CD32 antibody (2.4G2) from BD Biosciences.

Flow Cytometry

Tumor-bearing mice were sacrificed after the indicated treatment period and tissues processed by mechanical and enzymatic disruption to single-cell suspensions for immune cell profiling via flow cytometry. In order to exclude dead cells from analysis, live-dead cell staining with the LIVE/DEAD® Fixable Aqua Dead Cell Stain Kit (Invitrogen, Carlsbad, CA) was done according to the manufacturer's instructions prior to all other antibody staining. Antibody panel combinations used to distinguish immune cell populations were CD45^{+} (leukocytes) plus the following: SIINFEKL^{+} or CD169^{+} (SIINFEKL^{+} or CD169^{+} leukocytes); SIINFEKL^{+}, CD169^{+} (SIINFEKL^{+} CD169^{+} leukocytes); SIINFEKL^{+}, CD11b^{+}, F4/80^{+}, Gr-1^{-} (SIINFEKL^{+} macrophages); CD11b^{+}, F4/80^{+}, Gr-1^{-} (macrophages); SIINFEKL^{+}, CD11c^{+}, MHCII^{+}, F4/80^{-} (SIINFEKL^{+} dendritic cells); CD11c^{+}, MHCII^{+}, F4/80^{-} (dendritic cells); SIINFEKL^{+}, CD11b$^{+/-}$, CD11c$^{+/-}$ (SIINFEKL^{+} myeloid cell subsets); CD169^{+}, CD11b^{+}, F4/80^{+} (CD169^{+} macrophages); CD169^{+}, CD11c^{+}, MHCII^{+} (CD169^{+} dendritic cells); SIINFEKL^{+} CD169^{+}, CD11b^{+}, F4/80^{+} (SIINFEKL^{+} CD169^{+} macrophages); SIINFEKL^{+}, CD169^{+}, CD11c^{+}, MHCII^{+} (SIINFEKL^{+} CD169^{+} dendritic cells); CD3^{+} (T-cells); CD3^{+}, CD4^{+} (CD4^{+} T-cells); CD3^{+}, CD8^{+} (CD8^{+} T-cells); CD3^{+}, CD8^{+}, IFN-γ^{+} (IFN-γ secreting CD8^{+} T-cells); CD8^{+}, OVA-tetramer^{+} (OVA-specific CD8^{+} T-cells). Tetramer staining was done according to manufacturer's instructions (MBL International), except that tetramer incubation with cells was done for 1 hr instead of 30 min at room temperature. Cell samples were fixed in Cytofix buffer (BD Biosciences), diluted to 1% paraformaldehyde (PFA) in PBS-/-, and run within 24 hours

on either a FACScan or LSRII flow cytometer (BD Biosciences). All data were analyzed using FlowJo v10 software (TreeStar).

IFN-β and IFN-γ Stimulation of Ifi27l2a *in vitro*

NDL tumor cells were plated in 6-well tissue-culture treated plates at a concentration of 5 x 10^5 cells/well. The next day, media was changed to complete media (Gibco, #11995 containing 10% FBS and 1% penicillin-streptomycin) supplemented with either IFN-γ (#575302, BioLegend) or IFN-β1 (#581302, BioLegend) at 500 or 1000 U/mL in a final volume of 2 mL per well. Cells were incubated continuously for 24 h in a 37°C humidified chamber containing 5% CO_2, after which the cells were collected, counted and snap frozen in liquid nitrogen for submission to the UC Davis Real-Time PCR Research and Diagnostics Core Facility for quantification of *Ifi27l2a* expression via qPCR.

RNA Isolation for RNA-seq

NDL tumors were submitted to the UC Davis Comprehensive Cancer Center's Genomics Shared Resource (GSR) for isolation of total cellular RNA and subsequent RNA-seq analysis. Total cellular RNA was isolated from snap-frozen NDL tumor pieces using the TRIzol Reagent (Invitrogen) and a modified protocol that incorporates an additional extraction with phenol/chloroform/isoamyl alcohol (25:24:1, pH 4.3) followed by an additional clean-up with an RNeasy spin column (Qiagen). RNA concentration and purity were assessed with a NanoDrop 2000 Spectrophotometer (Thermo Scientific) and quality assessments were made using an Agilent 2100 Bioanalyzer (Agilent Technologies, Santa Clara, CA).

Cell Isolation and nucleic acid preparation for real-time quantitative PCR

Mice were treated as described in the "*in vivo* studies" section and euthanized on day 38. NDL tumors were harvested and processed to single cell suspensions through mechanical and enzymatic disruption, followed by magnetic bead isolation of $CD8^+$ T-cells and NDL tumor cells. $CD8^+$ T-cells were isolated from total cell samples using the negative-selection EasySep™ Mouse $CD8^+$ T-Cell Isolation Kit (Stemcell Technologies). NDL tumor cells were isolated from total cell samples using the negative-selection Tumor Cell Isolation Kit (Miltenyi Biotech). Isolated cell pellets were resuspended in 200 µl phosphate buffered saline (PBS) and then mixed with 200 µl of Buffer VXL + 20 µl Proteinase K. Two stainless steel grinding beads (4 mm diameter, SpexCertiprep, Metuchen, NJ) were added and the cells homogenized in a GenoGrinder2000 (SpexCertiprep) for 2.5 min at 1750 strokes per minute. Lysate was incubated for 10 minutes at 56°C. 200 µl of lysate was removed and used for total nucleic acid (TNA) extraction and the remaining saved as backup. TNA extraction was performed on a semi-automated extraction system (QIAcube, Qiagen) according to manufacturer's instructions. TNA was eluted in 100 µl of diethylpyrocarbonate-treated water.

Directional RNA-seq library preparation and next-generation sequencing

Indexed RNA-seq libraries were prepared using the NEBNext Ultra Directional RNA Library Prep Kit (New England BioLabs, Ipswich, MA), according to the manufacturer's standard protocol. Briefly, poly-adenylated mRNA was purified from total RNA (100 ng) and ribosomal RNA removed by binding to magnetic oligo$(dT)_{25}$ beads, which was followed by RNA fragmentation. Double-stranded cDNA was then generated by random-primed first-strand synthesis and subsequent second strand synthesis in the presence of dUTP for strand marking (*1, 2*). The double-stranded cDNA was then end repaired, 3'-dA tailed, and an Illumina-compatible NEBNext adaptor was ligated. Uridine excision was performed with the USER (Uracil-Specific Excision Reagent) enzyme, and the libraries were then indexed and enriched by high-fidelity PCR amplification (15 cycles) with Q5 High-Fidelity DNA Polymerase and NEBNext multiplex primers. Subsequently, libraries were combined for multiplex sequencing on an Illumina HiSeq 4000 System (150-bp, paired-end, ~25-30 x10^6 reads per sample).

NGS Data Analysis

RNA-seq data was analyzed using a STAR-StringTie-Cufflinks pipeline. De-multiplexed raw sequence reads (FASTQ format) were mapped to the reference mouse genome assembly (GENCODE, GRCm38, release 05/2017) using STAR (Spliced Transcripts Alignment to a Reference) software with a 2-pass alignment approach that uses initial alignment to detect novel junctions and insert them into the genome index, followed by a second pass to re-align reads using both annotated (GENCODE, Release M14, GRCm38.p5) and novel (detected in the first pass) junctions (*3*). Mapped reads were then passed onto StringTie for transcript assembly (*4*). Subsequently, gene- and transcript-level expression were comprehensively quantified with Cufflinks tools (*e.g.*, Cuffquant, Cuffnorm) to yield normalized expression as FPKM (fragments per kilobase of transcript per million fragments mapped reads) and test for differential expression (Cuffdiff).

NGS Data Processing

Cuffnorm files were imported to MATLAB for processing and analysis. Z-scores were calculated using raw FPKM values across all presented samples for a single gene. Principal component analysis was performed on the log2 transformed FPKM values using the singular value decomposition algorithm. Hierarchical clustering was performed using Euclidean pairwise distances and unweighted average cluster distances (UPGMA). Gene set enrichment analysis was performed on the set of all differentially expressed genes for each CuffDiff analysis (*i.e.,* genes with a differential expression at $p<0.01$) using DAVID's Functional Annotation Tool. Specifically, the GO Biological Processes and the KEGG Pathways were investigated (*5*).

RT-reaction and real-time TaqMan PCR

Real-time PCR was performed through the UC Davis Real-Time PCR Research and Diagnostics Core Facility. TaqMan Gene Expression Assays were ordered from Applied Biosystems (Carlsbad, CA) for murine Ki67 (Mm01278617_m1), Slc2a1 (Mm0044148_m1), Wnt7b (Mm01301717_m1), Ifi27l2a (Mm01329883_gH), Psrc1 (Mm00498358_m1), Pdcd1 (Mm01285676_m1), and the reference genes Ubc (Mm02525934_g1, for normalization in $CD8^+$ T-cell samples) and Actb (Mm00607939_s1, for normalization in tumor-cell samples). The 5′ end of the TaqMan MGB probes are labeled with FAM reporter dye, the 3′ end with quencher dye NFQMGB (Non-Fluorescent Quencher Minor Grove Binding). The Quantitect Reverse transcription kit (Qiagen) was used for cDNA synthesis following the manufacturer's directions with the following modifications. Ten µl of RNA were digested with 1 µl of gDNA WipeOut Buffer by incubation at 42°C for five minutes and then briefly centrifuged. Genomic DNA contamination was tested by using 1 µl of digested RNA and running the Real-time PCR housekeeping gene. Then 0.5 µl of Quantitect Reverse Transcriptase, 2 µl Quantitect RT buffer, 0.5 µl RT Primer Mix, 0.5 µl 20 pmol Random Primers (Invitrogen) were added and brought up to a final volume of 20 µl and incubated at 42°C for 40 minutes. The samples were inactivated at 95°C for 3 minutes, chilled, and 80 µl of water was added (*6*). Each qPCR reaction contained 20x primer and probes for the respective TaqMan system and commercially available PCR mastermix (TaqMan Universal PCR Mastermix, Applied Biosystems) containing 10 mM Tris-HCl (pH 8.3), 50 mM KCl, 5 mM $MgCl_2$, 2.5 mM deoxynucleotide triphosphates, 0.625 U AmpliTaq Gold DNA polymerase per reaction, 0.25 U AmpErase UNG per reaction and 5 µl of the diluted cDNA sample in a final volume of 12 µl. The samples were placed in 384 well plates, in singlet, and amplified in an automated real-time PCR System (ABI PRISM 7900 HTA FAST, ABI). ABI's standard amplification conditions were used: 2 min at 50°C, 10 min at 95°C, 40 cycles of 15 s at 95°C and 60 s at 60°C. Fluorescent signals were collected during the annealing temperature and Cq values extracted with a threshold of .2 and baseline values of 3-15 (*6*).

Relative quantitation of gene transcription

Final quantitation was done using the comparative Cq method (User Bulletin #2, Applied Biosystems) and is reported as relative transcription or the n-fold difference relative to a calibrator cDNA. In brief, the reference gene was used to normalize the Cq values of the target genes (ΔCq). The ΔCq was calibrated against the average of the control group within each target gene. The linear amount of target molecules relative to the

calibrator was calculated by $2^{-\Delta\Delta Cq}$. Therefore, all gene transcription is expressed as an n-fold difference relative to the calibrator.

SUPPLEMENTARY FIGURES

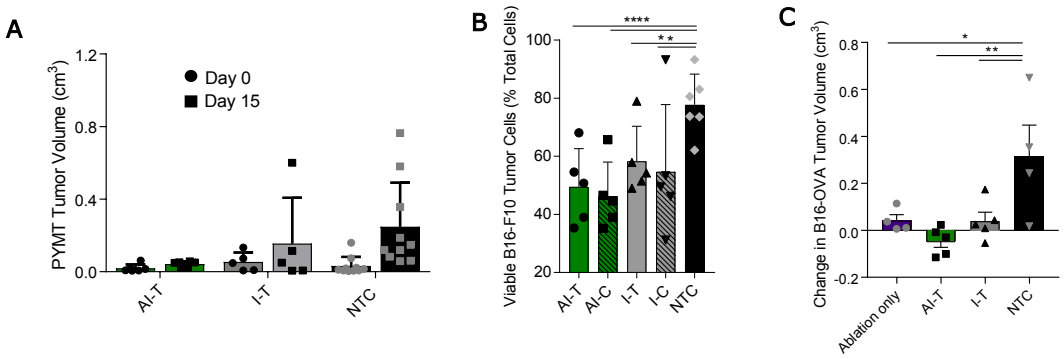

Supplementary Figure S1. Tumor response to AI treatment in NDL, PYMT, B16-OVA and B16-F10 models. (**A**) MMTV-PyVT transgene mice were treated once tumors reached approximately 5 mm in largest dimension (~10 weeks old). Mice were treated with the same protocol as in Fig. 1A. Groups included: AI (n=5), I (n=5), and NTC (n=5). (**B**) Coincident administration of thermal ablation, CpG, and anti-PD-1 was performed 13 days after B16-F10 cell injection, followed by a single injection of CpG on Day 16. Tumors were harvested on Day 19 for flow cytometry. Groups included: AI (n=5), I (n=5), and NTC (n=3). Tumors were processed to single cell suspensions and stained with Fixable Aqua Dead Cell stain for viability quantification via flow cytometry. (**C**) Consecutive dosing with immunotherapy was performed in C57BL/6 mice injected with B16-OVA tumor cells as indicated in Fig. 5A. Groups included: ablation only (n=4), AI (n=5), I (n=5), NTC (n=4). For the AI-T cohort, ablation was administered on day 11. Treatment commenced once tumors reached approximately 5 mm in largest diameter. Plots represent the change in tumor growth 48 hours after thermal ablation of a directly treated tumor. * $p < 0.05$, ** $p < 0.01$, ****$p < 0.0001$ (ANOVA with Fishers LSD test).

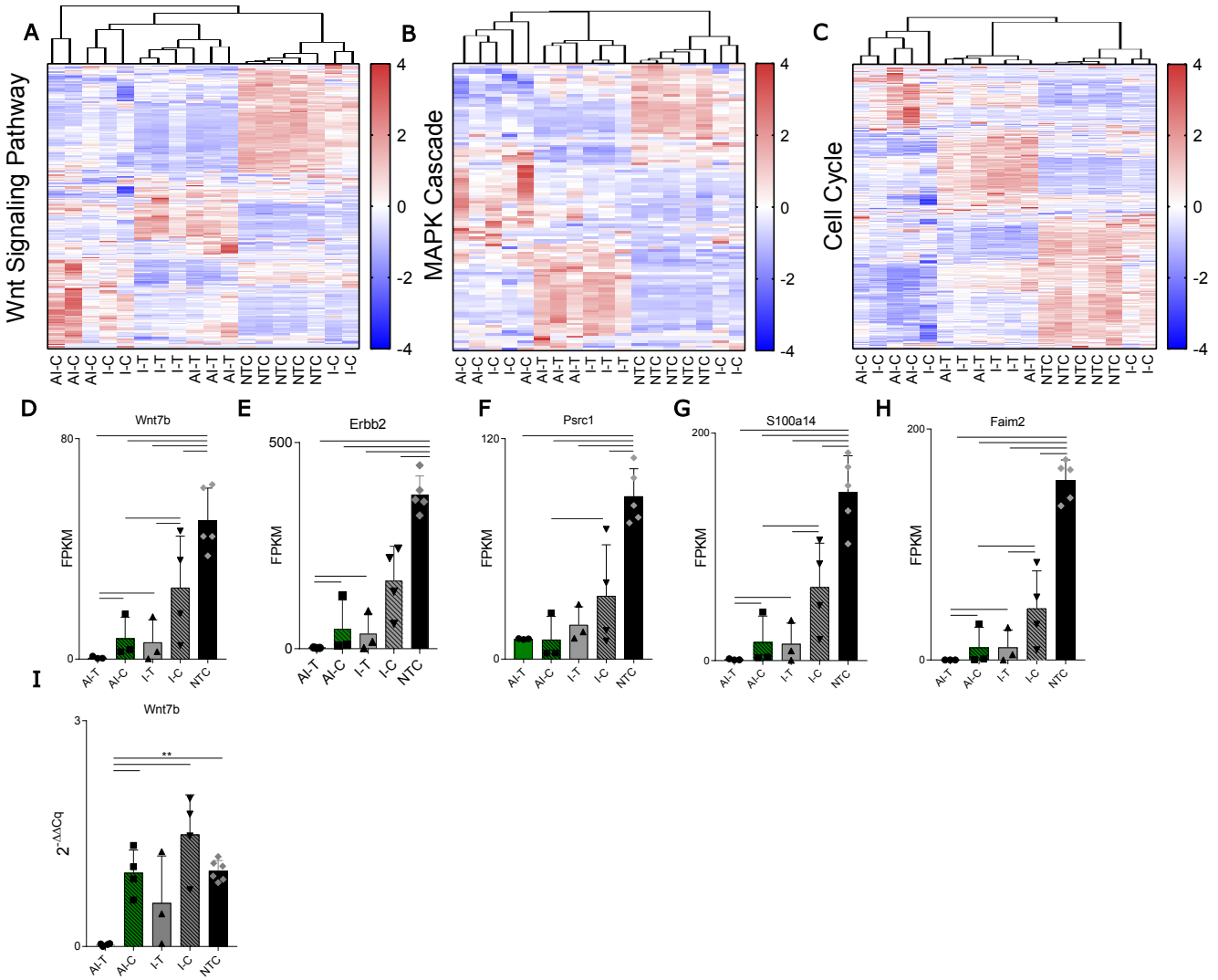

Supplementary Figure S2. RNA-seq and qPCR results for WNT, MAPK and cell cycle signaling. NDL mice treated as in Figure 1A. Biological groups for both RNA-seq and qPCR included ablation-immunotherapy (AI), immunotherapy-alone (I), and No Treatment Control (NTC), where treated tumors are denoted as either AI-T or I-T, and contralateral tumors are denoted as either AI-C or I-C. (**A-C**) Dendrograms of genes associated with (**A**) Wnt signaling, the (**B**) MAPK cascade and (**C**) cell cycle as generated from RNA-seq data. (**D**) Expression of the signaling protein essential to canonical Wnt signaling (*Wnt7b*), (**E**) *Erbb2*, a protein associated with HER2^{+} breast cancer, (**F**) *Psrc1*, a protein required for cellular progression through mitosis, and (**F-G**) the apoptosis inhibitors (**G**) *S100a14* and (**H**) *Faim2* as assessed by RNA-seq. (**I**) RNA levels of *Wnt7b* as measured by qPCR. All data plotted are mean ± SD. Dendrogram heatmaps are normalized by each gene using z-scores of the fragments per kilobase of transcript per million mapped reads (FPKM) values across all presented samples. For RNA-seq data, AI: n=3, 6 tumors; I: n=4, 7 tumors; NTC: n=5, 5 tumors. Bars represent significance of at least $p < 0.01$ as defined by CuffDiff. For qPCR data, AI: n=4, 8 tumors; I: n=5, 10 tumors; NTC: n=3, 6 tumors. **p<0.01 (ANOVA with Fishers LSD test).

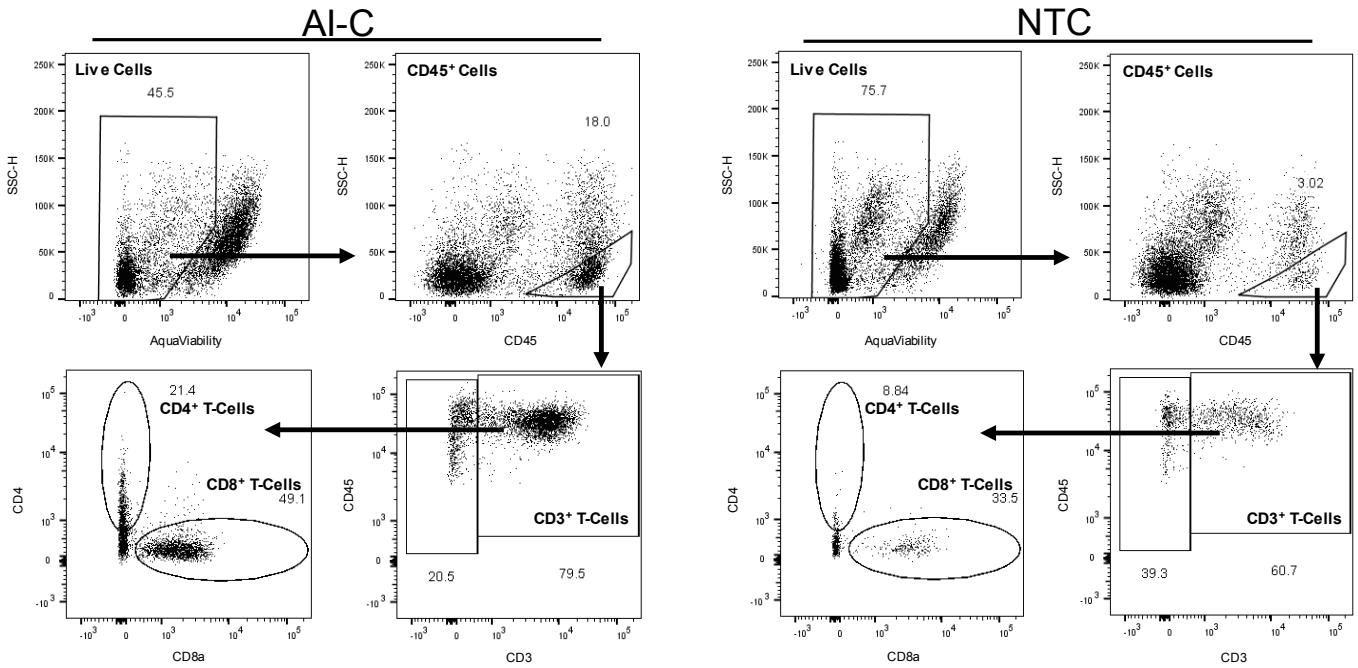

Supplementary Figure S3. T-cell flow cytometry gating strategy in NDL model (Figure 1A protocol), assayed at day 38. Gating strategy used in flow cytometric analysis for elucidating live cells, $CD3^+$ T-cells, $CD4^+$ T-cells, and $CD8^+$ T-cells.

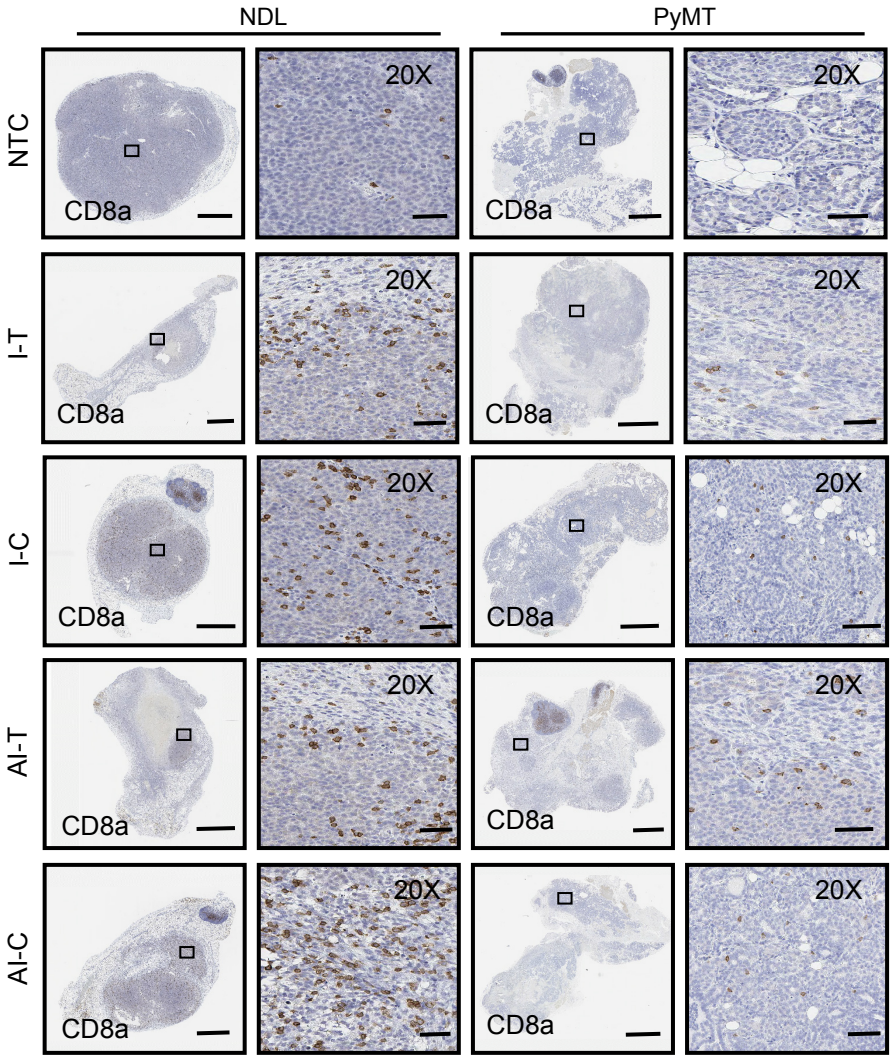

Supplementary Figure S4. Immunohistochemistry staining of intratumoral CD8$^+$ T-cells in NDL and PYMT tumors. Treatment as in Fig. 1A for NDL (beginning on day 21 after tumor implantation) and PyMT (beginning when tumors reached 0.5 cm in largest diameter) mice. Groups included: ablation-immunotherapy (AI), immunotherapy-alone (I), and No Treatment Control (NTC), where treated tumors are denoted as AI-T or I-T, and contralateral tumors are denoted as AI-C or I-C. CD8a IHC in treated and contralateral tumors in the PyMT and NDL models, respectively, as compared to NTC tumors. Scale bars are 2 mm for whole tumors and 80 μm for 20X images.

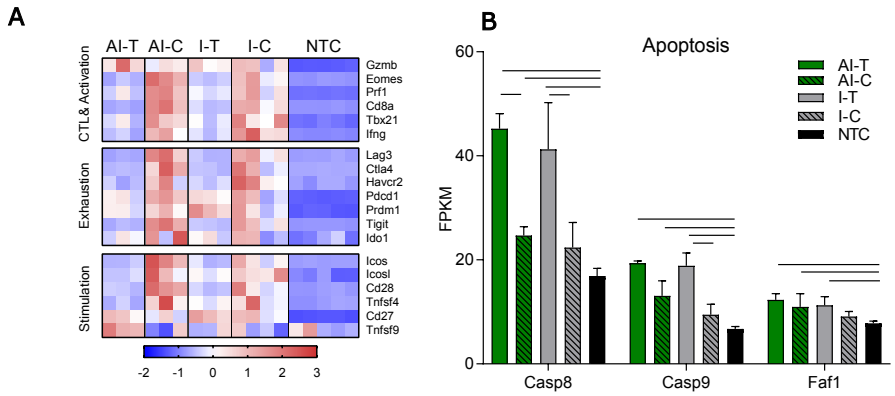

Supplementary Figure S5. Expression of activation, exhaustion, stimulation, and apoptotic T-cell markers. (**A**) RNA-seq results for cytotoxic T-cell and activation markers (first block), T-cell exhaustion markers (second block), and costimulatory checkpoints (third block). (**B**) RNA-seq results for genes associated with apoptosis (*Casp8*, *Casp9*, *Faf1*). Groups for RNA-seq of NDL tumor mice at day 38 as treated in Fig. 1A included: ablation-immunotherapy (AI), immunotherapy-alone (I), and No Treatment Control (NTC, n=5), where treated tumors are denoted as AI-T (n=3) or I-T (n=3), and contralateral tumors are denoted as AI-C (n=4), or I-C (n=4). All heatmaps are normalized by each gene using z-scores of the FPKM values across all presented samples. Bars represent significance of at least $p < 0.01$ as defined by CuffDiff.

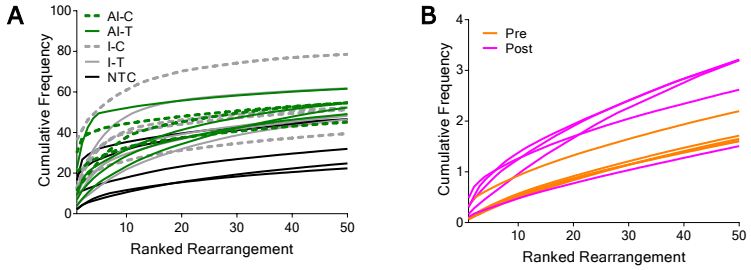

Supplementary Figure S6. Variability in the cumulative frequency of the top 50 clones. Groups for T-cell receptor sequencing (TCR-seq) of NDL tumor mice, as treated in Figure 1A, included: ablation-immunotherapy (AI, n=17 tumors), immunotherapy-alone (I, n=8 tumors), and No Treatment Control (NTC, n=11 tumors), where treated tumors are denoted as AI-T or I-T, and contralateral tumors are denoted as AI-C or I-C. Blood was harvested before (AI-Pre, n=5) or after AI treatment (AI-Post, n=5). Data represent two separate experiments and numbers indicate mouse number. (**A-B**) Cumulative frequency of the top 50 clones for (**A**) each tumor sample in the first experiment and (**B**) in blood before and after treatment.

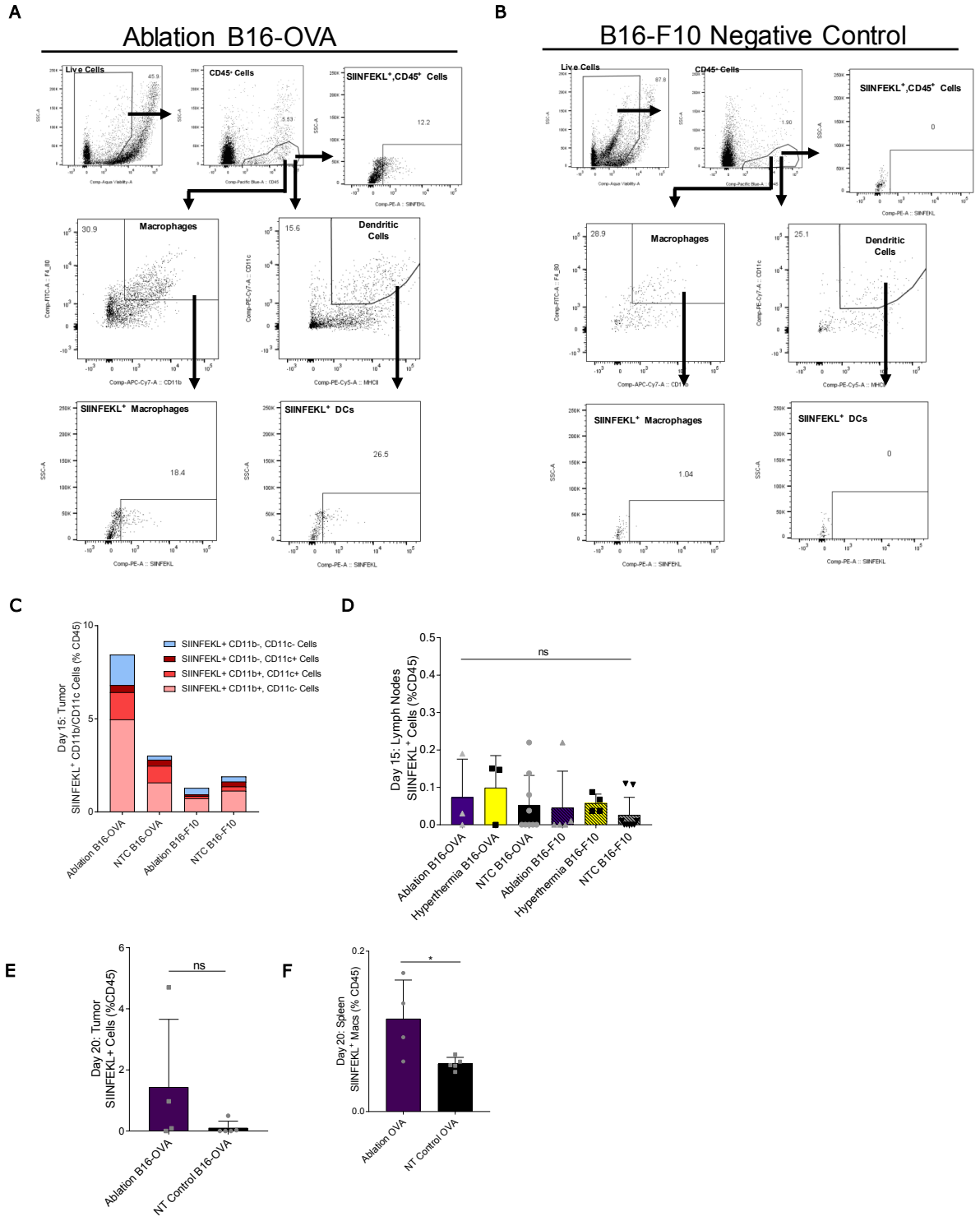

Supplementary Figure S7. Flow gating and results for SIINFEKL studies in B16-OVA/B16-F10 model. (**A-B**) Gating strategy used in flow cytometric analysis for elucidating SIINFEKL$^+$ antigen-presenting cells (APCs) in B16-OVA/B16-F10 bilateral tumor-bearing mice treated as in Figure 4A. Data shown obtained ~2 days after ablation. Gates shown represent the (**A**) ablated B16-OVA tumors and the (**B**) B16-F10 negative control used to determine SIINFEKL$^+$ leukocytes, macrophages and dendritic cells (DCs). (**C**) Intratumoral SIINFEKL$^+$ cells stratified into CD11b and CD11c subsets 48 hours after ablation. (**D**) Fraction of SIINFEKL$^+$ cells in the lymph nodes ~2 days after ablation. (**E-F**) Flow cytometry frequencies at ~7 days after ablation for (**E**) SIINFEKL$^+$ leukocytes in AI-T (n=4) and NTC (n=5) OVA tumors and (**F**) SIINFEKL$^+$ macrophages in the spleen. *p<0.05 (ANOVA with Fishers LSD test). All data plotted are mean ± SEM.

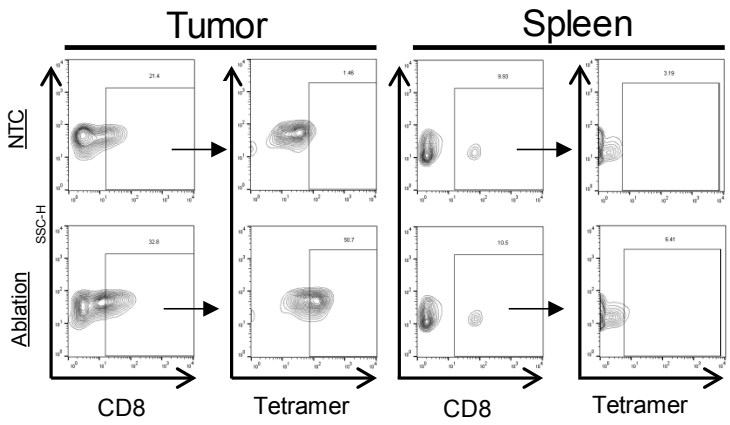

Supplementary Figure S8. Tetramer gating in B16-OVA model. Gating strategy used in flow cytometric analysis for elucidating Tetramer^{+} CD8^{+} T-cells in the tumor and spleen of B16-OVA unilateral tumor-bearing mice treated as in Figure 4A, assayed 7 days after ablation. Contour plots shown represent the gates used after gating on the fraction of live, CD45^{+} cells in ablated and No Treatment Control (NTC) B16-OVA tumors and spleens from ablated and NTC cohorts.

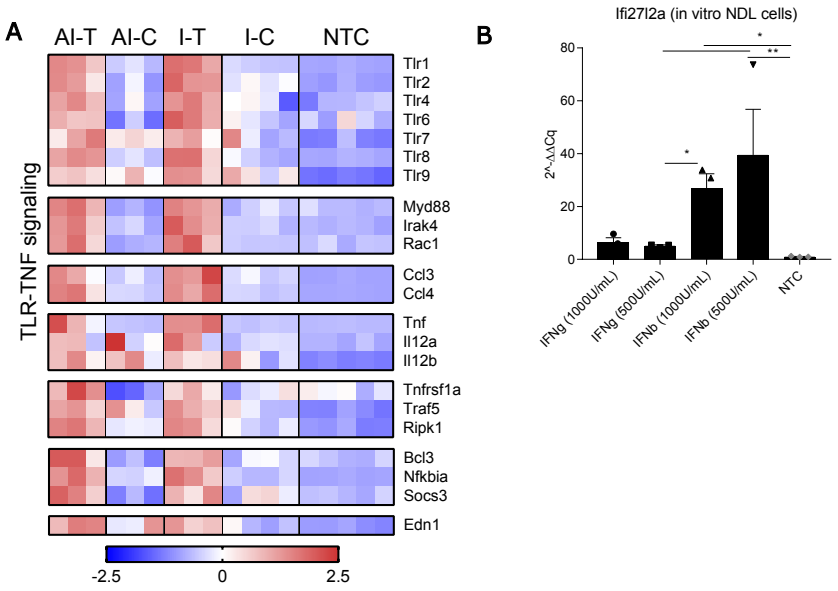

Supplementary Figure S9. Innate immune pathways upregulated in directly-treated tumors and *in-vitro* Ifi27l2a expression in NDL cells. Treatment as in Figure 1A for NDL mice, assayed at day 38. Biological groups included ablation-immunotherapy (AI, n=3, 6 tumors), immunotherapy-alone (I, n=4, 7 tumors), and No Treatment Control (NTC, n=5, 5 tumors), where treated tumors are denoted as either AI-T or I-T, and contralateral tumors are denoted as either AI-C or I-C. (**A**) RNA-seq results for expression of toll-like receptor (TLR) and TNF signaling genes upregulated with treatment. Heatmap is normalized by each gene using z-scores of the FPKM values across all presented samples. (**B**) Expression of the type I IFN integrating factor, *Ifi27l2a*, as measured by qPCR from isolated NDL cells *in vitro*. Samples included stimulation for 24 hrs with IFN-γ (1000U/mL), IFN-γ (500U/mL), IFN-β (1000U/mL), IFN-β (500U/mL), and no treatment control (NTC) (n=15, 3 per sample group). All data are presented as mean ± SD, where *p<0.05, **p<0.01, (ANOVA with Fishers LSD test).

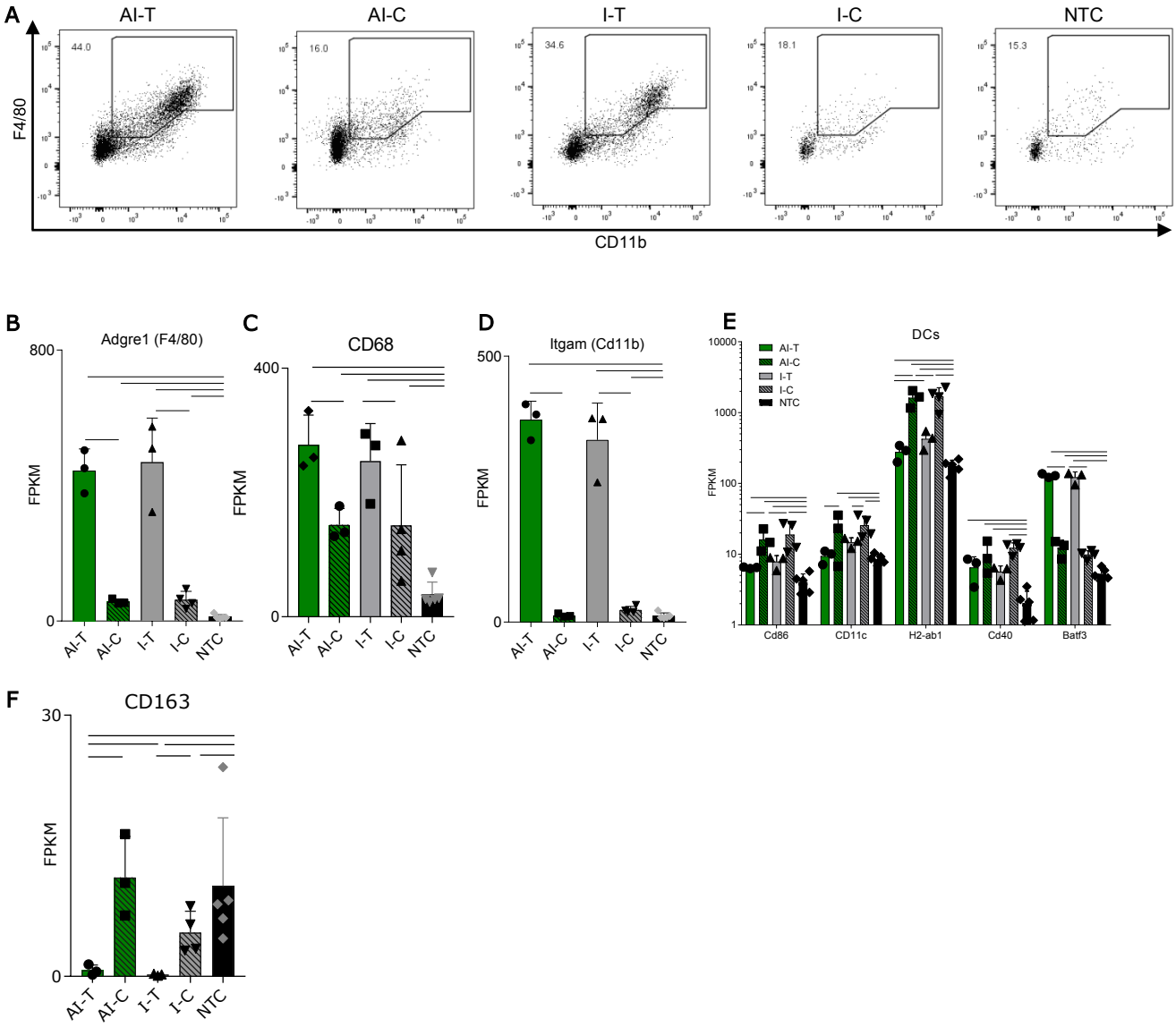

Supplementary Figure S10. Flow gating used to identify macrophages and RNA seq results for myeloid cell markers at Day 38. (**A**) Gating strategy used in flow cytometric analysis for elucidating $CD11b^{+}$, $F4/80^{+}$ macrophages (given as a fraction of live, $CD45^{+}$ cells) in the tumors of treated and no treatment control cohorts. (**B-E**) RNA-seq results for (**B**) associated macrophage markers *Adgre1* (F4/80), (**C**) *Cd68*, (**D**) *Itgam* (*CD11b*). (**E**) important DC markers including *Cd86*, *Cd11c*, *H2-ab1*, *Cd40,* and *Batf3*. (**F**) Phenotypic marker *Cd163*. AI: n=3, 6 tumors; I: n=4, 7 tumors; NTC: n=5, 5 tumors. Data plotted as mean ± SD, where bars represent significance of at least $p < 0.01$ as defined by CuffDiff.

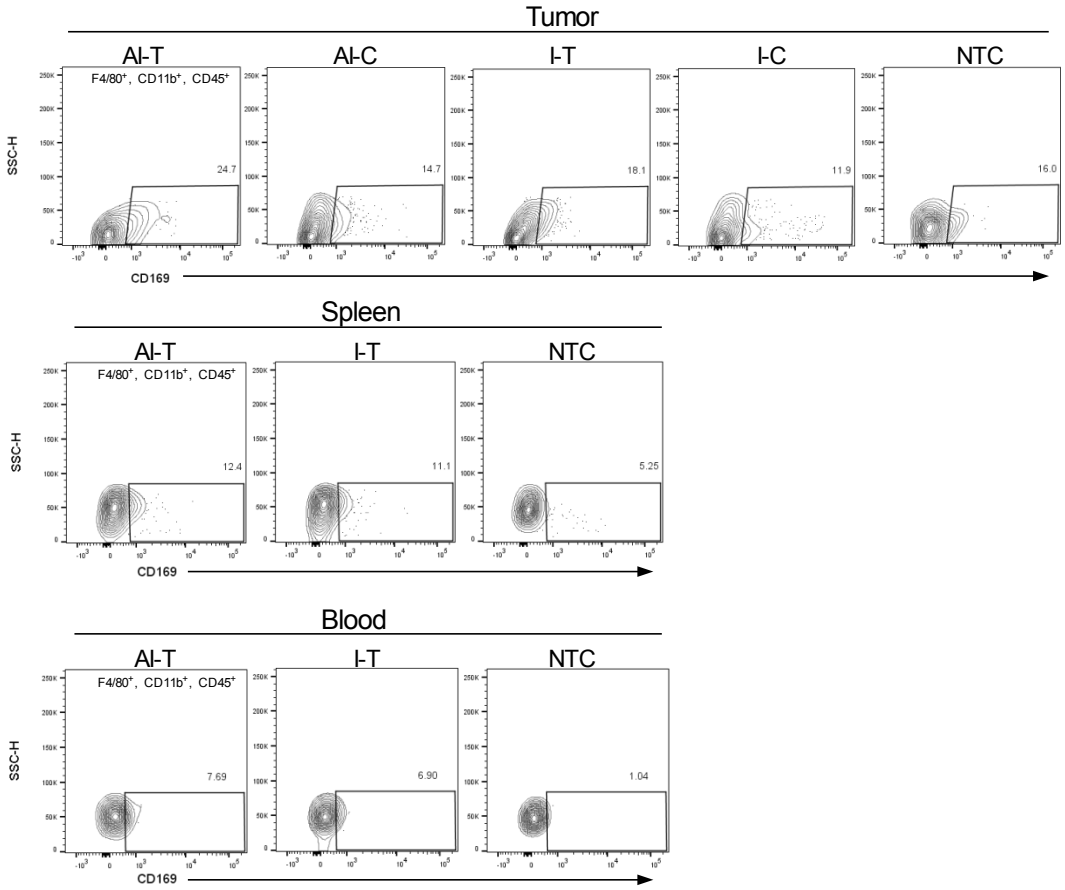

Supplementary Figure S11. CD169$^+$ macrophage flow cytometry gating. Gating strategy used in flow cytometric analysis for elucidating CD169$^+$ macrophages (F4/80$^+$, CD11b$^+$, CD45$^+$ cells) in the tumor, spleen, and blood of NDL mice treated as in Figure 1A and assayed 3 days after ablation (Day 34).

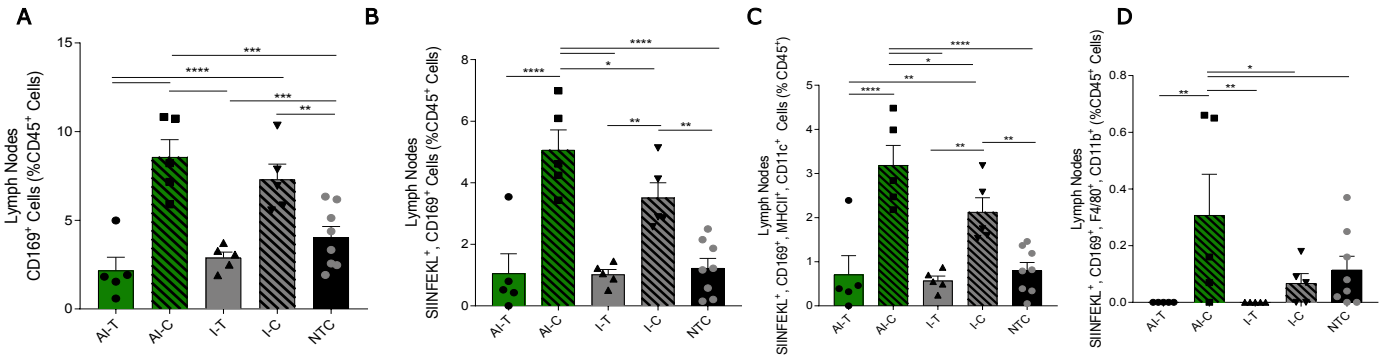

Supplementary Figure S12. Expression of CD169$^+$, SIINFEKL$^+$ cells in B16-OVA model after AI treatment using protocol in Fig. 5A. Groups included: ablation-immunotherapy (AI, n=5), immunotherapy-alone (I, n=5), and No Treatment Control (NTC, n=4), where treated tumors and their associated draining lymph nodes are denoted as either AI-T or I-T, and contralateral (distant) lymph nodes are denoted as either AI-C or I-C. Tumors, spleen, draining and contralateral (distant), lymph nodes were harvested for flow cytometric quantification at Day 14 after tumor cell injection. (**A**) Frequency of CD169$^+$ leukocytes in the lymph nodes 72 hours after treatment. (**B**) Percentage of SIINFEKL$^+$, CD169$^+$ leukocytes in the lymph nodes after treatment. (**C-D**) Frequencies of (**C**) dendritic cells and (**D**) macrophages that are double positive for both SIINFEKL and CD169 in the lymph nodes. *p<0.05, **p<0.01, *** p <0.001, **** p <0.0001 (ANOVA with Fishers LSD test). All data plotted are mean ± SEM.

Supplementary Table S1. Annotations for AI-T upregulated with respect to I-T regarding the innate immune response.

Category	Term	Annotation	Count	%	PValue	Genes	List Total	Pop Hits	Pop Total	Fold Enrichment	Bonferroni	Benjamini	FDR
GOTERM_BP_DIRECT	GO:0070098	chemokine-mediated signaling pathway	14	2.868852459	2.94E-10	CCL2, CXCL5, CCR1, CXCL3, CXCL2, CCL9, PF4, ACKR3, CXCL12, CCL7, CCL6, CCL11, CCL12, PPBP	422	55	18082	10.9068505	6.74E-07	1.35E-07	5.13E-07
GOTERM_BP_DIRECT	GO:0006935	chemotaxis	18	3.68852459	2.04E-09	RARRES2, CCL2, CXCL5, CCR1, CXCL3, S100A9, CXCL2, CCL9, PF4, ACKR3, CXCL12, CCL7, CCL6, LSP1, CCL11, CCL12, S1PR1, PDGFRA	422	118	18082	6.536187646	4.69E-06	7.82E-07	3.57E-06
GOTERM_BP_DIRECT	GO:0050729	positive regulation of inflammatory response	12	2.459016393	1.98E-07	CCL11, CCL12, ACE, CCL2, IL1RL1, S100A9, SERPINE1, CCL9, FABP4, ADAM8, CCL7, CCL6	422	63	18082	8.161588806	4.55E-04	3.04E-05	3.47E-04
GOTERM_BP_DIRECT	GO:0009615	response to virus	12	2.459016393	3.86E-06	IFIT3, IFIT1, ACTA2, OASL2, IFI27L2A, OASL1, RSAD2, OAS1A, OAS2, EIF2AK2, MX1, MX2	422	84	18082	6.121191605	0.008826432	3.85E-04	0.006745609
GOTERM_BP_DIRECT	GO:0030593	neutrophil chemotaxis	11	2.254098361	4.20E-06	CCL11, CCL12, CCL2, PPBP, CXCL3, S100A9, CXCL2, CCL9, TREM1, CCL7, CCL6	422	69	18082	6.830894979	0.009591642	4.02E-04	0.007333227
GOTERM_BP_DIRECT	GO:0006955	immune response	21	4.303278689	6.36E-06	IL6, CCL2, CXCL5, CCR1, CXCL3, CXCL2, MCPT4, CCL9, PF4, OAS2, CXCL12, CCL7, CCL6, CCL11, CCL12, CD36, PPBP, OASL2, OASL1, CMA1, OAS1G	422	272	18082	3.308143992	0.014497371	5.84E-04	0.011111158
GOTERM_BP_DIRECT	GO:0006954	inflammatory response	24	4.918032787	6.38E-06	IL6, RARRES2, CCL2, PTGS2, CXCL5, CCR1, CXCL3, S100A9, CXCL2, CCL9, EPHX2, PF4, CXCL12, CCL7, CCL6, CD163, CCL11, CCL12, S1PR3, AGTR2, LTB4R1, CHIL3, TPSB2, ADAM8	422	344	18082	2.989419156	0.014536554	5.63E-04	0.011141408
GOTERM_BP_DIRECT	GO:0048247	lymphocyte chemotaxis	7	1.43442623	9.99E-05	CCL11, CCL12, CCL2, CCL9, ADAM8, CCL7, CCL6	422	33	18082	9.08904208	0.204957918	0.005578534	0.174367748
GOTERM_BP_DIRECT	GO:0022617	extracellular matrix disassembly	6	1.229508197	1.27E-04	LAMA3, NID1, LAMC1, MMP3, LAMB1, MMP13	422	22	18082	11.68591125	0.252650733	0.006749737	0.221345654
GOTERM_BP_DIRECT	GO:0051607	defense response to virus	14	2.868852459	1.50E-04	IL6, RSAD2, OAS2, IFIT3, IFIT1, ISG15, OASL2, OASL1, OAS1A, SPON2, MX1, EIF2AK2, OAS1G, MX2	422	167	18082	3.59207651	0.291344594	0.00762381	0.261699815
GOTERM_BP_DIRECT	GO:0001938	positive regulation of endothelial cell proliferation	9	1.844262295	1.58E-04	CCL11, ARG1, CDH13, VEGFD, CAV1, CCL2, ANG, CXCL12, KDR	422	67	18082	5.75574733	0.305057722	0.007880232	0.276528217
GOTERM_BP_DIRECT	GO:0002523	leukocyte migration involved in inflammatory response	5	1.024590164	1.75E-04	CCL2, PPBP, S100A9, ADAM8, AOC3	422	13	18082	16.48013124	0.331383118	0.008528194	0.30582672
GOTERM_BP_DIRECT	GO:0030334	regulation of cell migration	9	1.844262295	4.18E-04	MMP10, LAMA4, LAMA3, TEK, DPYSL3, MMP3, CXCL12, THY1, EPHA3	422	77	18082	5.008247676	0.616885399	0.01640568	0.72736427
GOTERM_BP_DIRECT	GO:0060326	cell chemotaxis	9	1.844262295	4.56E-04	NOV, CCL12, CCL2, CXCL5, CXCL2, PDGFRA, CCL9, CXCL12, CCL6	422	78	18082	4.944039373	0.64927045	0.017601553	0.794054698
GOTERM_BP_DIRECT	GO:0030595	leukocyte chemotaxis	5	1.024590164	0.001519269	S1PR1, CCR1, S100A9, CXCL2, PF4	422	22	18082	9.738259371	0.969526375	0.047328023	2.621250005
GOTERM_BP_DIRECT	GO:0010744	positive regulation of macrophage derived foam cell differentiation	4	0.819672131	0.001799001	LPL, MSR1, CD36, PF4	422	11	18082	15.58121499	0.983984934	0.05433596	3.09676426
GOTERM_BP_DIRECT	GO:0019221	cytokine-mediated signaling pathway	11	2.254098361	0.002241583	CCL12, IL1R1, IL6, BGN, CCL2, EREG, IL1RN, PF4, DCN, PTPRN, LRRC15	422	146	18082	3.228299682	0.994214793	0.064725257	3.844637527
GOTERM_BP_DIRECT	GO:0002548	monocyte chemotaxis	6	1.229508197	0.002247404	CCL11, CCL12, CCL2, CCL9, CCL7, CCL6	422	40	18082	6.427251185	0.994291767	0.064083291	3.854437191
GOTERM_BP_DIRECT	GO:0050927	positive regulation of positive chemotaxis	4	0.819672131	0.002357456	CDH13, S1PR1, F7, KDR	422	12	18082	14.28278041	0.995568905	0.066296471	4.039538354
GOTERM_BP_DIRECT	GO:0045087	innate immune response	20	4.098360656	0.002767958	S100A9, RSAD2, SERPING1, OAS2, FCGR1, IFIT3, IFIT1, ANG, OASL2, IRF7, OASL1, OAS1A, PTX3, EIF2AK2, CFD, MX1, SPON2, C1S1, SSC5D, MX2	422	400	18082	2.142417062	0.998277612	0.074675033	4.727019618
GOTERM_BP_DIRECT	GO:0090026	positive regulation of monocyte chemotaxis	4	0.819672131	0.003767872	CCL2, CCR1, SERPINE1, CXCL12	422	14	18082	12.24238321	0.99982789	0.095871173	6.382228538
GOTERM_BP_DIRECT	GO:0002690	positive regulation of leukocyte chemotaxis	4	0.819672131	0.004629208	PPBP, CXCL5, PF4, F7	422	15	18082	11.42622433	0.999976378	0.112813844	7.786269355
GOTERM_BP_DIRECT	GO:0071346	cellular response to interferon-gamma	7	1.43442623	0.004986264	CCL11, MRC1, CCL12, CCL2, CCL9, CCL7, CCL6	422	68	18082	4.410858656	0.999989635	0.118492679	8.36245537
GOTERM_BP_DIRECT	GO:0002675	positive regulation of acute inflammatory response	3	0.614754098	0.013798908	IL6, ADAM8, AOC3	422	8	18082	16.06812796	1	0.240446971	21.55315575
GOTERM_BP_DIRECT	GO:0002687	positive regulation of leukocyte migration	4	0.819672131	0.013892363	CCL12, CCL2, MMP9, AOC3	422	22	18082	7.790607497	1	0.240073986	21.68292532
GOTERM_BP_DIRECT	GO:0002376	immune system process	17	3.483606557	0.01807084	S100A9, RSAD2, SERPING1, OAS2, FCGR1, IFIT3, IFIT1, OASL2, IRF7, OASL1, SPON2, C1S1, MX1, CFD, EIF2AK2, MX2, SSC5D	422	383	18082	1.901884598	1	0.284633949	27.28258099
GOTERM_BP_DIRECT	GO:0007229	integrin-mediated signaling pathway	7	1.43442623	0.021472865	ADAMTS19, ADAMTS14, COL3A1, FERMT2, ADAM33, ADAM19, ADAM8	422	93	18082	3.225143964	1	0.322513078	31.56065424
GOTERM_BP_DIRECT	GO:0048246	macrophage chemotaxis	3	0.614754098	0.040910157	CCL12, EDNRB, CCL2	422	14	18082	9.181787407	1	0.474633177	51.7966191
GOTERM_BP_DIRECT	GO:0050829	defense response to Gram-negative bacterium	5	1.024590164	0.041215053	LALBA, CHGA, ADM, SERPINE1, SSC5D	422	56	18082	3.825744753	1	0.474935556	52.06363174
GOTERM_BP_DIRECT	GO:0050900	leukocyte migration	4	0.819672131	0.044031639	ANG, CD34, MMP9, TEK	422	34	18082	5.040981321	1	0.484571157	54.46518102
KEGG_PATHWAY	mmu04062	Chemokine signaling pathway	14	2.868852459	9.61E-04	CCL2, CXCL5, CCR1, CXCL3, CXCL2, CCL9, PF4, CXCL12, CCL7, CCL6, CCL11, CCL12, PPBP, SHC2	189	196	7720	2.917611489	0.162161915	0.019466958	1.181730872
KEGG_PATHWAY	mmu04610	Complement and coagulation cascades	8	1.639344262	0.002405529	PLAT, F13A1, SERPINE1, SERPING1, F7, CFD, C1S1, PLAUR	189	76	7720	4.299637984	0.357989467	0.04334749	2.933572239
KEGG_PATHWAY	mmu04060	Cytokine-cytokine receptor interaction	15	3.073770492	0.002564986	IL1R1, IL6, CCL2, CCR1, PF4, ACKR3, CXCL12, CCL7, KDR, CCL11, LEP, CCL12, VEGFD, PPBP, PDGFRA	189	245	7720	2.500809848	0.376597972	0.042050611	3.12520756
KEGG_PATHWAY	mmu05168	Herpes simplex infection	12	2.459016393	0.012577857	CCL12, FOS, IFIT1, IL6, CCL2, IRF7, PER1, OAS1A, OAS2, ARNTL, EIF2AK2, OAS1G	189	208	7720	2.356532357	0.902607248	0.143813368	14.48532936
KEGG_PATHWAY	mmu05162	Measles	9	1.844262295	0.017758362	IL6, IRF7, CD209F, CD209G, OAS1A, OAS2, EIF2AK2, OAS1G, MX2	189	136	7720	2.703081232	0.963002313	0.167365996	19.86950883
KEGG_PATHWAY	mmu05164	Influenza A	10	2.049180328	0.023684855	CCL12, IL6, CCL2, IRF7, RSAD2, OAS1A, OAS2, EIF2AK2, OAS1G, MX2	189	171	7720	2.388687769	0.987850319	0.207156218	25.64592132
KEGG_PATHWAY	mmu05144	Malaria	5	1.024590164	0.028815935	CCL12, IL6, CCL2, CD36, THBS2	189	48	7720	4.254850088	0.995392293	0.235857699	30.33525318

Supplementary Table S2. Animal numbers and biological groups across all studies.

Study	Mouse Strain	Tumor Model	Biological Group	Time point	Number
Immunohistochemistry and blood ELISA	C57BL/6	B16-F10/B16-F10	NTC	Day 15	4
			Ablation		2
	FVB/n	NDL	NTC	Day 31	4
			AI		4
			NTC	Day 38	9
			Immunotherapy		9
			AI		9
	FVB/N-Tg(MMTV-PyVT)634Mul/J	PyMT	NTC	Tumors of 0.5 cm were treated for 17 days	5
			Immunotherapy		6
			AI		3
SIINFEKL Studies	C57BL/6-Tg(CAG-OVA)916Jen/J	N/A	Positive Control	Day 15	4
	C57BL/6	B16-F10/B16-F10	Negative Control		4
		B16-F10/B16-OVA	NTC		15
			Ablation		5
			Hyperthermia		4
CD169 SIINFEKL		B16-OVA	NTC	Day 14	4
			Immunotherapy		5
			AI		5
SIINFEKL/Tetramer Study			NTC	Day 20	5
			Ablation		4
RNAseq Studies	FVB/n	NDL	NTC	Day 38	5
			Immunotherapy		4
			AI		4
qPCR Studies	FVB/n	NDL	NTC	Day 38	3
			Immunotherapy		5
			AI		5
TCRseq Studies	FVB/n	NDL	NTC	Day 38	8
			Immunotherapy		5
			AI		11
Flow cytometry	FVB/n	NDL	NTC	Day 34	3
			Immunotherapy		4
			AI		4
			NTC	Day 38	6
			Immunotherapy		8
			AI		8
Total NDL					118
Total C57BL/6 or CagOVA					61
Total PyMT					14
Total					193

SUPPLEMENTARY REFERENCES

1. T. Borodina, J. Adjaye, M. Sultan, A strand-specific library preparation protocol for RNA sequencing. *Methods Enzymol* **500**, 79-98 (2011).
2. J. Z. Levin *et al.*, Comprehensive comparative analysis of strand-specific RNA sequencing methods. *Nat Methods* **7**, 709-715 (2010).
3. A. Dobin, T. R. Gingeras, Mapping RNA-seq Reads with STAR. *Curr Protoc Bioinformatics* **51**, 11 14 11-11 14 19 (2015).
4. M. Pertea *et al.*, StringTie enables improved reconstruction of a transcriptome from RNA-seq reads. *Nat Biotechnol* **33**, 290-295 (2015).
5. D. W. Huang, B. T. Sherman, R. A. Lempicki, Systematic and integrative analysis of large gene lists using DAVID bioinformatics resources. *Nat. Protocols* **4**, 44-57 (2008).
6. N. Pusterla, S. Mapes, W. D. Wilson, Diagnostic sensitivity of nasopharyngeal and nasal swabs for the molecular detection of EHV-1. *Vet Rec* **162**, 520-521 (2008).